名古屋大学博物館報告
Bull. Nagoya Univ. Museum
No. 38, 1–21, 2023
DOI: 10.18999/bulnum.038.01

Geochemistry and K-Ar age of the mafic rocks at the Uubulan area, Khangai-Daur belt, Central Asian Orogenic belt, central Mongolia

Bayart NADMID[1)]*, Kazuhiro TSUKADA[2)], Munkhtsetseg OIDOV[3)], Sharav DAVAANYAM[4)], Manchuk NURAMKHAAN[5)], Lodoidanzan ALTANSUKH[3)], Khishigbadam DAVGADORJ[3)], and Kanta UMEDA[6)]

1）Department of Earth and Planetary Sciences, Graduate School of Environmental Studies, Nagoya University, Furo-cho, Chikusa-ku, Nagoya 464-8601, Japan
2）Nagoya University Museum, Furo-cho, Chikusa-ku, Nagoya 464-8601, Japan
3）Department of Geology and Hydrogeology, School of Geology and Mining, MUST main building, 8th khoroo, Baga toiruu, Sukhbaatar district, Ulaanbaatar, 14191, Mongolia
4）Institute of Geology, Mongolian Academy of Sciences, Trade Union Street, 18th khoroo, Songinokhairkan district, Ulaanbaatar, 18080, Mongolia
5）Academic Affairs, Branch of Mongolian University of Science and Technology, Division of Erdenet Mining Co., Erdenet, Mongolia
6）Technical Planning and Coordination Department, Japan Petroleum Exploration Co., Ltd., Marunouchi, Chiyoda-ku, Tokyo, 100-0005, Japan
**Corresponding author:* Bayart Nadmid (n.bayart@yahoo.com)

Abstract

This paper describes the whole-rock geochemical composition, clinopyroxene (Cpx) chemical composition, and the hornblende K-Ar age of the mafic rocks in the Carboniferous accretionary complex of the Khangai-Daur belt, Central Asian Orogenic belt, exposed at the Uubulan area of Mongolia. The geochemical nature of the mafic rocks, enriched in large ion lithophile elements and light rare-earth elements compared with high field-strength elements (HFSE) and heavy rare-earth elements, suggest that they are alkaline basalts. The $(La/Yb)_{cn}$ vs. HFSE diagrams show that the samples are oceanic island basalts. Therefore, the mafic rocks are concluded to be oceanic-island alkaline basalts. The comparatively high concentrations of Al, Ti, Na, and Ca in the Cpx of the mafic rocks strongly support this view. The mafic rocks just beside the Upper Silurian radiolarian chert give a hornblende K-Ar age of 412.7 ± 8.6 Ma. The fact that Upper Silurian chert strongly suggests that the oceanic-island alkaline basalts are conformably underlain by the radiolarian chert formed at the pelagic region as a base of oceanic plate stratigraphy.

Keywords: Mafic rocks, K-Ar age, Carboniferous accretionary complex, Khangai-Daur belt, Central Asian Orogenic belt.

Introduction

The Central Asian Orogenic belt (CAOB: Jahn *et al*., 2004; Xiao *et al*., 2003; Windley *et al*., 2007; Petrov *et al*., 2014) is the largest Paleozoic–Mesozoic orogenic belt in the world (Fig. 1a). The development process of the CAOB, which lies among the Siberian craton, East European craton, Tarim block, and North China block (Sengör *et al*., 1993), is essential to understand the tectonic history of the Eurasian continent (Kovalenko *et al*., 2004). The CAOB is generally considered to have been formed by the subduction-accreation process of the oceanic plate, magmatism of a volcanic arc magmatism, and collisions of continental fragments during the amalgamation of

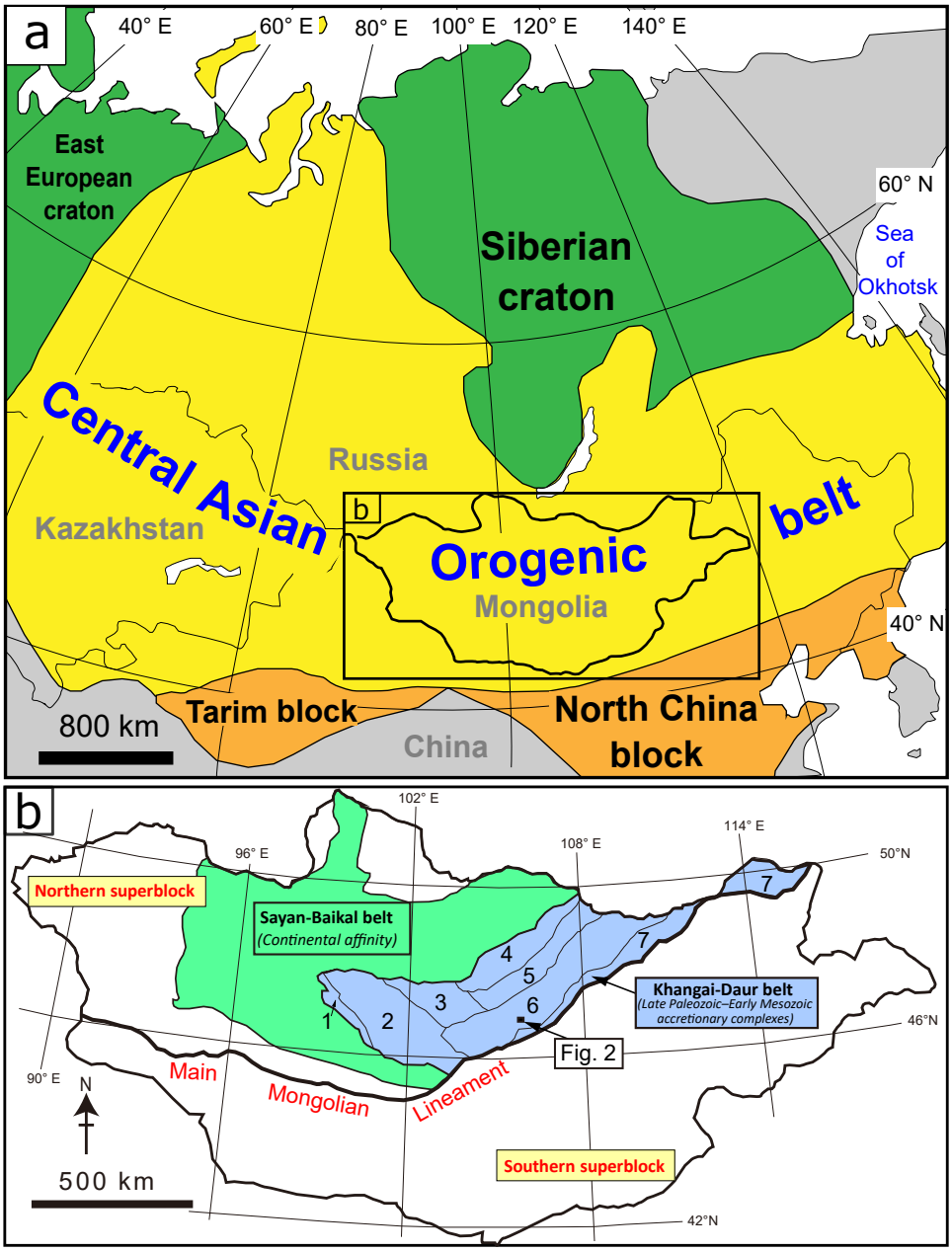

Fig. 1 a) Index map (modified from Petrov *et al*., 2014); b) simplified tectonic division of northern Mongolia: 1, Zag terrane; 2, Tsetserleg terrane; 3, Kharhorin terrane; 4, Kharaa terrane; 5, Asralt-Khairhan terrane; 6, Ulaanbaatar terrane; 7, Onon terrane. Modified from the study by Badarch *et al*. (2002), Tomurtogoo (2003), and Tsukada *et al*. (2018).

these cratons and blocks (Sengör *et al*., 1993).

The geological information of Mongolia, between the North China block and the Siberian craton, offers a key to understanding the Paleozoic–Mesozoic tectonics of the southern margin of the "Siberian continent (Siberian craton + accreted geologic units)" at southern CAOB. Further, the general features of the Khangai-Daur (also spelled as Hangay-Hentey or Khangai-Hentei or Khangai-Khentei or Hangai-Daur) and Sayan-Baikal belts, a significant constituent of northern Mongolia, has been substantially established (Badarch *et al*., 2002; Tomurtogoo, 2003; Kurihara *et al*., 2009; Onon, 2017 MS; Onon and Tsukada, 2017: Fig. 1b).

The Khangai-Daur belt has been subdivided into the following seven geologic units: Kharaa, Zag, Tsetserleg, Kharhorin, Asralt-Khairhan, Onon, and Ulaanbaatar terranes (Tomurtogoo, 2012; Onon and Tsukada, 2017:

Fig. 1b). The Kharaa and Zag terranes are composed mostly of shelf facies rocks, and others are of accretionary complexes (Onon and Tsukada, 2017). Onon (2017 MS) pointed out that the Kharaa and Zag terranes are similar to the Sayan-Baikal belt rather than the other terranes of the Khangai-Daur belt in lithostratigraphy and excluded these terranes from the Khangai-Daur belt to incorporate them into the Sayan-Baikal belt. This paper regards the rocks of the Tsetserleg, Kharhorin, Asralt-Khairhan, Onon, and Ulaanbaatar terranes as the component of the Khangai-Daur belt, following Onon (2017 MS).

The Khangai-Daur belt is composed mainly of clastic rocks with minor amounts of radiolarian chert, siliceous mudstone, mafic rocks, and limestone (Tomurtogoo *et al*., 1998, Badarch *et al*., 2002; Tomurtogoo, 2003; Kurihara *et al*., 2009; Takeuchi *et al*., 2012; Tsukada *et al*., 2013; Ruppen *et al*., 2013; Onon and Tsukada, 2017). Kurihara *et al*. (2009) revealed that the Ulaanbaatar terrane consists of the Late Paleozoic accretionary complex formed by the subduction of the previous oceanic plate, and they established Late Silurian to Late Devonian oceanic-plate stratigraphy (OPS) in the Gorkhi Formation, Ulaanbaatar terrane, based on radiolarian biostratigraphy.

The OPS can provide key information regarding the continuous evolution of oceanic plates (Matsuda and Isozaki, 1991; Wakita and Metcalfe, 2005). Kurihara *et al*. (2009) recovered Late Silurian conodonts from the chert beside the mafic rocks exposed at the Uubulan area to define the basal part of the OPS in the Gorkhi Formation (Figs. 2 and 3). Although the mafic rocks have been presumed to be Upper Silurian because of the conodont from the chert, its precise age has not been revealed. Additionally, the mafic rocks were estimated to have an affinity of oceanic alkaline basalt by X-ray fluorescence (XRF) analysis (Tsukada *et al*., 2013); however, more accurate geochemical data is required to clarify its detailed geochemical feature.

The geochemistry and age of the mafic rocks, which is the lowermost unit of OPS, in the accretionary complex is an important factor in understanding the evolution of ancient oceanic-plates.

This paper describes the lithology, detailed whole-rock chemical composition, clinopyroxene (Cpx) chemical composition, and hornblende K-Ar age of the mafic rocks beside the Upper Silurian chert of the Gorkhi formation at the Uubulan area and discusses its tectonic setting and OPS position.

Geological outline

Mongolia is geologically divided into the northern and southern superblocks by the Main Mongolian Lineament. The Khangai-Daur belt in the northern superblock, approximately 300 km wide and 1200 km long, is mostly composed of Late Paleozoic accretionary complexes (Tomurtogoo, 2003; Onon 2017 MS) (Fig. 1b).

The accretionary complex of the Khangai-Daur belt is divided into the following five geological units: Tsetserleg, Kharhorin, Asralt-Khairhan, Onon, and Ulaanbaatar terranes (Onon 2017 MS). The Ulaanbaatar, Kharhorin, and Tsetserleg terranes are composed of Late Paleozoic accretionary complexes (Kurihara *et al*., 2009; Purevjav and Roser 2012; Tsukada *et al*., 2013) (Fig. 1b). The Asralt-Khairhan terrane is considered a metamorphosed part of the Ulaanbaatar terrane (Tomurtogoo 2012; Gordienko *et al*., 2012). The Onon terrane consists of deformed and metamorphosed accretionary complexes, fragments of ophiolite, and minor arc-related volcanic rocks (Bulgatov and Gordienko 1999; Zorin, 1999; Badarch, 2005; Tomurtogoo, 2012).

The rocks of the Ulaanbaatar terrane are subdivided into the following five geological units from south to north: Unegt, Sergelen, Dov, Gorkhi, and Altan-Ovoo & Orgioch-Uul formations (Dorjsuren *et al*., 2006; Minjin *et al*., 2006; Kurihara *et al*., 2008; Takeuchi *et al*., 2012; Sharav *et al*., 2019) (Fig. 2). The Unegt, Sergelen, and Dov formations are of deformed and metamorphosed clastic rocks and chert (Sharav *et al*., 2019). Generally, the metamorphism of the rocks is strong in the south, Sergelen Formation, and relatively weak toward the north to

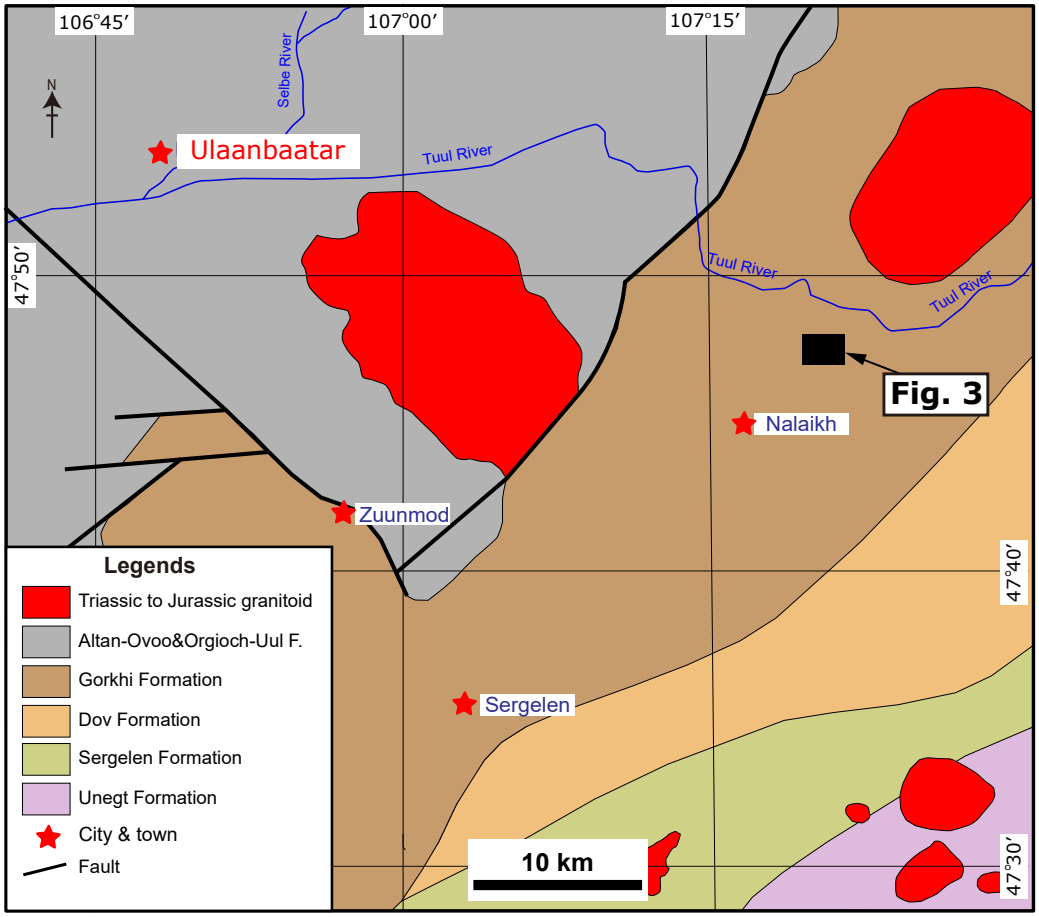

Fig. 2 Simplified geologic map of the Ulaanbaatar area. The geological division follows that of Dorjsuren *et al*. (2006). F.: Formation.

the Dov Formation (Sharav *et al*., 2019). The Gorkhi Formation comprises Upper Silurian to Upper Devonian radiolarian cherts, along with siliceous mudstone and clastic rocks. The Altan-Ovoo & Orgioch-Uul Formation consists mostly of sandstone, mudstone, and conglomerate with a minor amount of chert and felsic tuff (Nakane *et al*., 2012; Suzuki *et al*., 2012; Takeuchi *et al*., 2012).

Tsukada *et al*. (2013) showed that the mafic rocks in the Gorkhi Formation are oceanic-island alkaline rocks. Kurihara *et al*. (2009) reported Upper Silurian to Upper Devonian radiolarians and conodonts from the chert in the Gorkhi Formation. Kelty *et al*. (2008), Bussien *et al*. (2011), and Hara *et al*. (2013) assumed that the sandstone of the Gorkhi Formation was formed after the earliest Carboniferous based on detrital zircon chronology. Hara *et al*. (2013) mentioned that the geochemical data of the sandstone and mudstone of this formation suggests a continental margin or continental island-arc environment.

The Gorkhi Formation is probably unconformably overlain by the Carboniferous shallow marine formation, yielding bryozoans and brachiopods (Takeuchi *et al*., 2012), and intruded by the Triassic to Jurassic granitoid, showing biotite K-Ar ages of 220–205 Ma (Magic Project 1998; Gerel and Lkamsuren 1999).

Geological description at the Uubulan area

At Uubulan, southeast of Ulaanbaatar city, the mafic rocks and chert of the Gorkhi Formation are exposed (Figs. 3 and 4).

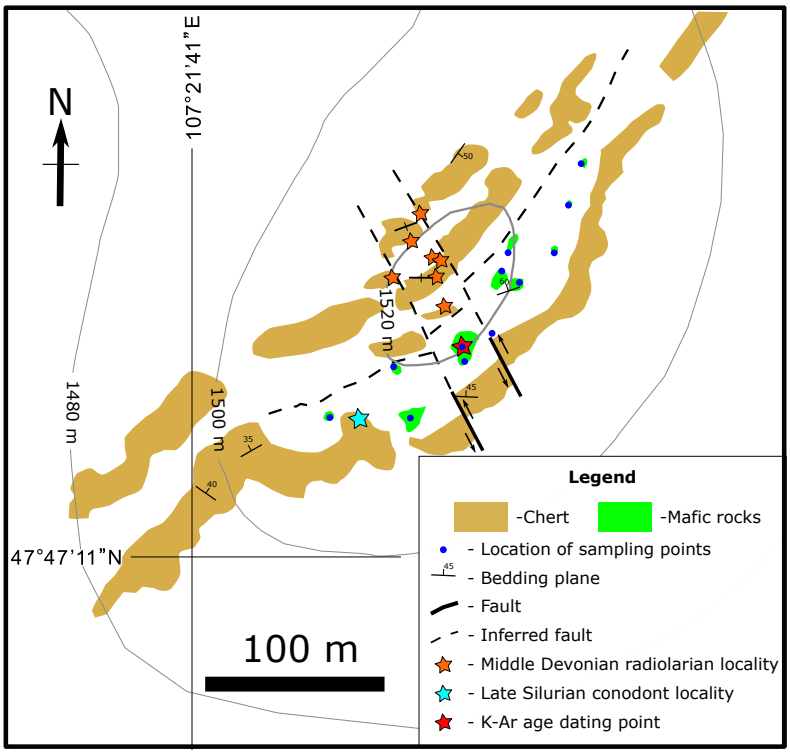

Fig. 3 Route map showing outcrops of the mafic rocks and chert of the Gorkhi Formation at the Uubulan area with sampling points for geochemical examination (blue circle) and dating (red star). Microfossil locations are indicated by orange and sky-blue stars.

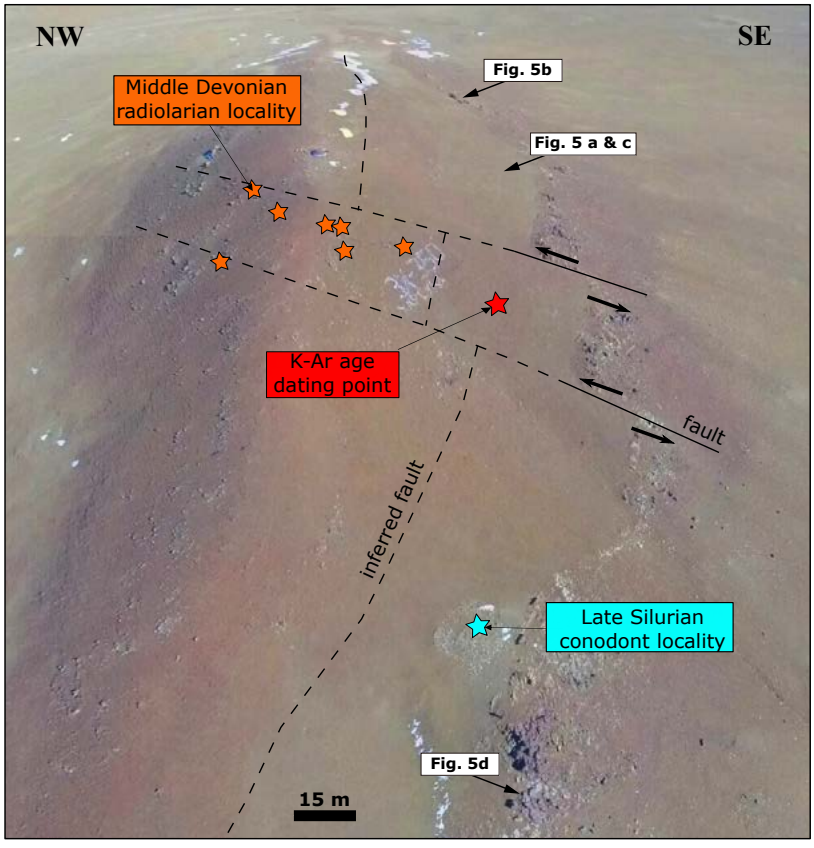

Fig. 4 Aerial view of the Uubulan area from the southwest, showing outcrops of chert and mafic rocks.

Red chert, trending NE–SW and steeply dipping north or south, is exposed at the north and south of the mafic rocks of dolerite, and gabbro (Fig. 5 a–d). South of the mafic rocks, the gray/reddish gray impure chert (gray tuffaceous chert in Kurihara *et al*., 2009) is covered by gray and red bedded radiolarian chert and overlain by massive chert. The bedded chert (approximately 5–7 cm thick in a bed) is folded and commonly cut by quartz veins. The conodonts suggesting Upper Silurian were reported from the red bedded chert (Kurihara *et al*., 2009). Red, gray/reddish gray chert is exposed near the peak of the hill, north of the mafic rocks. Middle Devonian radiolarian assemblage was obtained from the chert (Kurihara *et al*., 2009). The mafic rocks are probably in fault contact with the Middle Devonian red, gray/reddish gray chert.

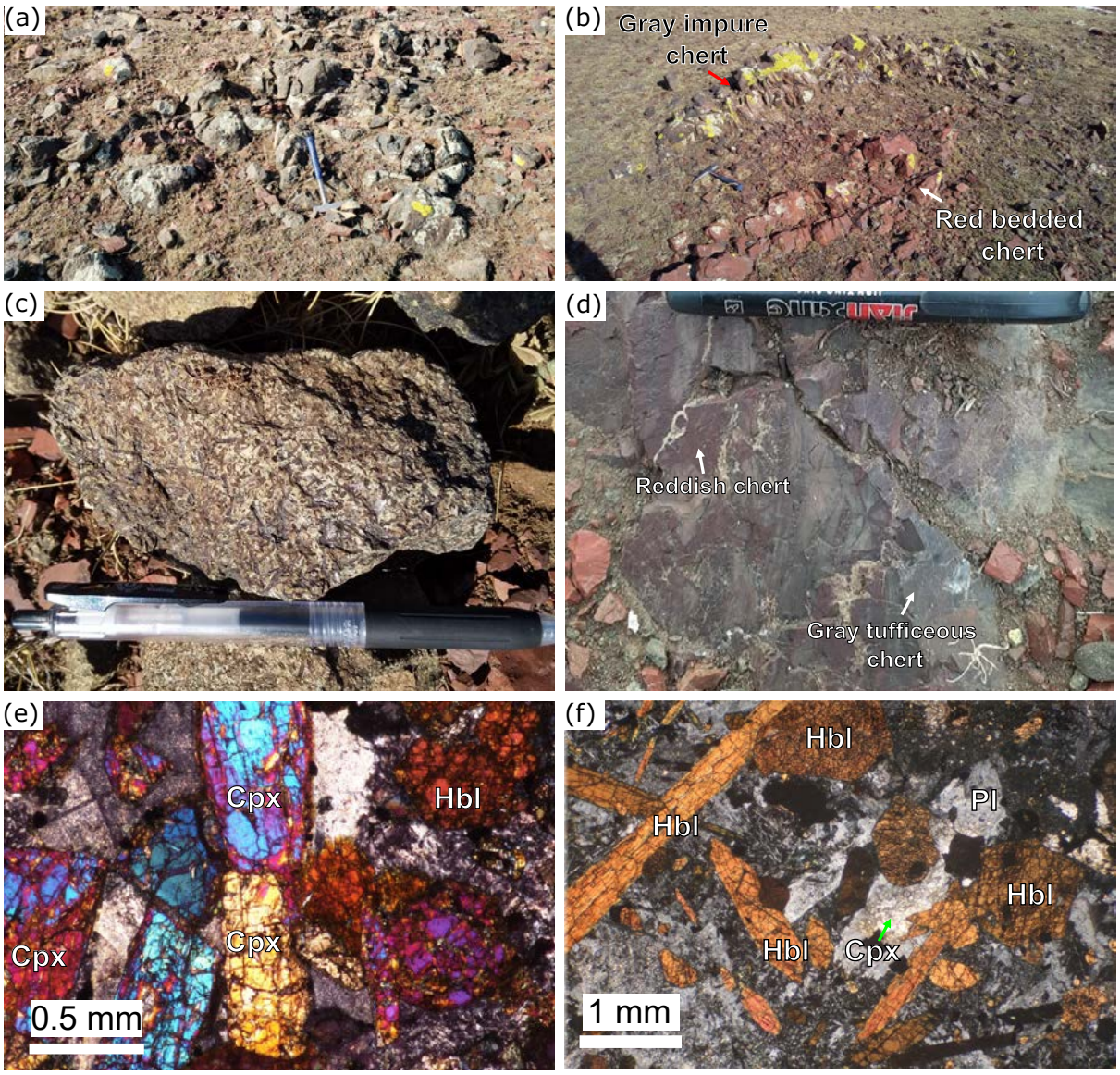

Fig. 5 Field photographs and photomicrographs of the rocks in the Uubulan area: (a) field occurrence of dolerite, (b) gray impure and red bedded chert, (c) close-up of the medium-grained dolerite, (d) the gray/reddish gray impure chert, (e) the photomicrograph of the Cpx-dominant dolerite, and (f) the photomicrograph of the hornblend-dominant dolerite/gabbro. Cpx: clinopyroxene; Hbl: hornblende; Pl: plagioclase calcite.

Among the mafic rocks in this area, dolerite is dominant, followed by gabbro. The relationship among them is unclear because of poor exposure. The dolerite, showing ophitic or spinifex-like texture, consists of euhedral plagioclase, hornblende, and anhedral Cpx (Fig. 5e). Minor amounts of opaque minerals are included. The gabbro is hypocrystalline and consists of medium to coarse-grained (>1 mm) plagioclase, hornblende, and Cpx (Fig. 5f). The hornblende is euhedral, dark brown. The Cpx is anhedral.

Methodology

1.1 Whole-rock chemical composition analysis

The dolerite samples were coarse-crushed using a steel bowl and pounder. After the coarse crushing, altered parts and veins were removed from all samples under a stereomicroscope. Each sample was >100 g. The concentrations of the major elements and Th were determined using XRF (Rigaku Primus II ZSX equipped with Rh X-ray tube, 50 kV, 60 mA), and trace elements, except for Th, and rare earth elements (REE) were analyzed by quadrupole-type inductively coupled plasma–mass spectrometry (ICP–MS; Agilent 7700x with collision cell of He) at Nagoya University.

For the XRF analysis, the glass beads were prepared by fusing mixtures of 1.5 g of powdered sample with 6.0 g of lithium tetraborate for the major elements and Th analysis. Calibration was conducted using standard rock samples issued by the Geological Survey of Japan and the composite standards prepared by Yamamoto and Morishita (1997). The analytical precision of the major elements was estimated to be <1% for Si and approximately 3% for other elements, except for CaO, MgO, and Na_2O, whose analytical precision was >3% when the measured level was <0.1% (Takebe and Yamamoto, 2003), and that for trace element was estimated to be less than 10% (Yamamoto and Morishita, 1997).

Most trace elements and REE composition were determined using ICP–MS with a technique based on the methodology described by Yamamoto *et al*. (2005). Approximately 30 mg of each sample was digested with a mixed solution of HF–$HClO_4$ (2:1 by volume) at 150°C. After the acids had completely evaporated, 2 mL of 1.7 N HCl was added to dissolve the cake. Thereafter, the residue was separated by centrifugation at 12,000 rpm using a 2-mL polypropylene tube. After centrifugation, the supernatant was transferred to another 10-mL Teflon beaker, and the residue was again fused with HF–$HClO_4$ (2:1 by volume) at 150°C. Afterward, the fused cake was dissolved with approximately 2 mL of 1.7 N HCl by mild heating, and the resulting solution was centrifuged at 12000 rpm. No residue was observed after centrifugation in most cases. Subsequently, the HCl solution was evaporated to dryness, and the fused cake was redissolved in a 2% HNO_3 solution and analyzed using ICP–MS. In and Bi were used to trace ICP sensitivities, and the In and Bi concentrations were mostly identical throughout the analysis. The oxide generation factor (LnO/Ln) was determined for each 20 ppb solution and used for REE analytical data correction. In the ICP–MS analysis, the correlation coefficients (R values) of each element, calculated for five standard samples, were 0.9994–1.0000, and the concentration relative standard deviation of the data was mostly < 3%.

1.2 Mineral chemical composition analysis

The Cpx chemical composition in the samples was determined using a method described by Tsukada (2018) using energy-dispersive X-ray spectrometer (EDX, Oxford X-Max) linked with scanning electron microscope (SEM, Hitachi S-3400N) at Nagoya University. The SEM-EDX analyses were performed with an acceleration voltage of 15 kV, analytical time of 40 seconds, and a working distance of 10 mm. Quartz (for Si) and augite (for

Ti, Al, Fe, Mg, Ca, and Na) were used for analytical standards. The total values of each analysis were normalized as 100%, following Tsukada (2018). The analytical precision of the analysis was estimated to be <5% when the measured level was more than 1 wt%, and <10% when the measured level was less than 1 wt% (Tsukada, 2018). Elements with a concentration of less than 0.5 wt% may not have been detected (Tsukada, 2018).

1.3 Hornblende K-Ar dating

The hornblende in the sample for the K-Ar dating was observed, and a significant alteration was not recognized (Fig. 5f). The sample was coarse-crushed using a steel bowl and pounder. Afterward, the hornblende was concentrated using heavy liquid (Na polytungstate solution) and ferrite and neodymium magnets.

The K-Ar dating was performed by the Hiruzen Institute for Geology and Chronology, Japan. Approximately 50 mg of hornblende, powdered in an agate mortar, was placed in a Teflon container and decomposed with HNO_3, FH, and H_2O_2 in a closed system box for more than 12 hours. After decomposition, the sample solution was evaporated to dryness in a closed system, and thereafter, the fused cake was re-dissolved with HCl for analysis. The analysis was performed using a flame atomic absorption spectrometer (Hitachi 180-30).

Ar isotope ratio was measured using a mass spectrometer (HIRU, Itaya *et al*., 1991) by isotope dilution method (Nagao *et al*., 1984; Nagao and Itaya, 1988; Itaya *et al*., 1991). Approximately 50 mg of sample was used for the analysis. The sample was evacuated at approximately 180°C to 200°C for three days to remove the adsorbed Ar. After reducing the background in the analytical system, the sample was dissolved at approximately 1500°C. The gas extracted from the sample was mixed with the spike (nearly 100% pure ^{38}Ar). The gas other than inert gas was removed using a Ti-Zr getter, and the purified gas was introduced into the mass spectrometer.

Analytical results

1.4 Whole-rock geochemical characteristics of the mafic rocks

Major elements, trace elements, and REE compositions of the mafic rocks from the Uubulan area are listed in Table 1. The SiO_2 concentration of the samples is 44.5–48.9 wt%. The loss of ignition (LOI) is <3.3 wt% for most samples.

In variation diagrams (Fig. 6), the examined samples have nearly identical TiO_2, Al_2O_3, Fe_2O_3, MnO, P_2O_5, V, Cr, Co, Hf, Ni, Zn, Ta, Pb, Zr, Nb, and Y concentrations. Na_2O and Sr increase and MgO and CaO decrease against increasing SiO_2. A mid-ocean ridge basalt (MORB)-normalized multi-element pattern (called “spidergram” hereinafter) shows enrichment in large ion lithophile elements (LILE) compared to high-field strength elements (HFSE) (Fig. 7). In the chondrite-normalized REE patterns, it is observed that samples are enriched in light rare-earth elements (LREE) and decrease toward heavy rare-earth elements (HREE) (Fig. 8).

Table 1 Whole-rock chemical composition of the mafic rocks from the Uubulan area. The data are displayed in three significant digits except for MnO and P_2O_5.* Fe_2O_3 total iron as Fe_2O_3. **trace element analyzed by XRF.

Sample No.	0508218163a	0508218163b	0508218163c	0508218163d	0508218163e	0508218164f	0508218163g	608197180	608197181	608197182	608197183	608197184	608197185	608197186	608197187	608197188	608197189	608197190	608197191	2019615B6	2019615B7	2019615B10
Major elements (wt%)																						
SiO_2	46.0	45.2	46.8	45.7	45.1	45.8	46.7	46.0	48.9	46.0	45.7	47.9	47.7	44.5	48.0	48.1	47.4	46.8	46.5	45.5	45.5	46.9
TiO_2	3.34	3.34	3.26	3.20	3.27	3.29	3.37	3.04	3.25	3.40	3.00	3.29	3.24	3.03	3.23	3.29	3.32	3.23	3.06	3.13	3.09	4.01
Al_2O_3	15.8	16.1	15.4	16.3	16.1	16.2	16.5	12.2	14.2	16.3	12.2	15.2	14.9	11.9	15.4	15.3	15.0	16.2	15.2	14.8	11.1	16.9
Fe_2O_3*	12.6	12.9	11.9	12.3	12.6	12.3	13.0	9.0	12.4	14.3	11.5	12.2	12.7	14.0	12.5	13.4	12.7	12.3	10.8	10.5	9.0	15.8
MnO	0.17	0.19	0.17	0.18	0.18	0.18	0.20	0.14	0.21	0.19	0.15	0.18	0.19	0.16	0.20	0.28	0.19	0.21	0.18	0.17	0.15	0.29
MgO	6.24	6.18	6.09	5.54	6.25	5.69	6.77	7.55	5.53	6.37	7.41	4.50	4.95	8.16	4.36	4.50	4.65	6.67	4.35	4.47	8.96	5.72
CaO	10.4	10.3	10.5	10.6	10.2	10.1	6.40	16.6	9.39	6.73	15.2	10.0	8.37	14.0	9.65	8.83	10.0	6.45	13.4	13.6	17.9	6.61
Na_2O	3.24	3.26	3.16	2.75	2.97	2.94	3.42	2.38	4.54	3.12	2.58	4.28	4.92	2.33	4.70	4.23	4.24	3.21	3.52	3.33	1.90	2.35
K_2O	1.46	1.48	1.93	2.36	2.20	2.24	2.78	2.08	0.94	2.88	1.33	1.75	1.05	1.11	1.42	1.44	1.52	3.33	2.68	2.85	1.00	1.48
P_2O_5	0.75	0.74	0.88	0.88	0.77	0.90	0.78	0.47	0.64	0.88	0.45	0.74	0.74	0.48	0.74	0.77	0.74	0.79	0.71	0.71	0.47	0.64
Total	**99.9**	**99.7**	**100**	**99.9**	**99.6**	**99.6**	**100**	**99.4**	**100**	**100**	**99.5**	**99.9**	**98.7**	**99.6**	**100**	**100**	**99.7**	**99.2**	**100**	**97.2**	**99.0**	**101**
LOI	2.97	3.25	3.12	3.54	4.05	3.37	3.72	5.27	1.56	3.62	3.47	0.87	1.42	3.18	2.12	1.96	2.08	3.59	5.60	6.24	3.60	4.67
Trace elements (ppm)																						
V	297	289	265	233	269	255	267	319	282	261	316	280	266	342	230	245	284	251	273	230	312	156
Cr	26.6	13.9	60.9	9.45	9.60	11.3	8.51	489.6	296	6.97	801	76.6	71.6	769	54.8	73.3	79.3	12.7	40.1	25.2	409	57.4
Co	39.0	41.1	33.0	32.5	36.5	35.6	39.5	40.7	43.4	40.2	31.5	32.4	34.7	35.6	31.2	35.5	31.8	37.7	30.3	31.6	34.4	38.0
Ni	45.9	56.8	36.4	32.3	40.1	34.5	40.6	78.4	77.5	34.5	83.7	43.1	41.7	101.1	39.0	45.9	41.8	39.9	40.0	37.4	93.3	83.3
Zn	114	116	108	116	135	122	123	73.0	118	124	82.2	125	120	90.1	114	194	122	137	135	95.6	68.9	155
Rb	23.9	23.5	27.5	32.7	27.0	29.3	39.7	49.0	23.2	42.8	33.3	55.2	24.3	28.7	29.9	37.6	46.4	43.4	66.4	58.9	24.7	23.2
Sr	559	613	538	508	549	514	696	456	592	556	550	1180	941	438	889	762	1091	653	757	638	354	553
Y	27.7	26.9	29.6	31.6	27.7	29.7	27.6	27.2	24.9	27.3	25.6	27.2	28.6	25.6	29.2	32.7	33.0	28.0	27.0	24.9	31.3	41.1
Zr	257	248	261	257	250	259	208	223	217	199	214	245	241	225	236	263	243	209	234	238	238	209
Nb	70.7	72.8	69.6	76.0	74.1	75.0	79.2	39.5	58.0	79.3	40.2	70.5	69.2	43.0	69.4	67.3	69.4	76.1	66.1	64.3	38.2	47.6
Ba	503	539	472	483	491	552	691	616	331	631	236	388	306	353	337	518	298	676	435	472	176	256
Pb	20.4	4.89	3.17	4.19	3.56	4.94	3.48	2.23	3.73	3.41	2.51	3.76	4.02	2.48	4.18	14.65	4.62	2.63	6.05	3.46	1.65	3.58
Hf	6.23	5.71	6.19	5.85	5.76	5.81	5.06	6.33	5.41	4.83	6.06	5.62	5.67	6.25	5.66	6.07	5.97	5.23	5.60	6.07	7.54	5.99
Ta	5.65	5.69	5.54	5.90	5.74	5.60	6.03	3.43	4.39	6.23	3.43	5.32	5.31	3.72	5.50	5.39	5.55	6.11	5.36	4.46	3.00	3.48
Th**	12.1	3.90	5.80	4.80	9.50	11.0	9.30	11.6	17.7	9.80	8.20	12.3	13.9	8.30	12.1	12.8	9.20	14.0	9.90	9.00	5.00	10.0
Rare earth elements (ppm)																						
La	43.2	43.7	44.9	52.1	44.1	48.3	44.3	28.4	36.3	48.3	28.7	43.3	43.3	29.2	46.3	45.7	50.2	48.1	41.3	39.1	28.1	30.0
Ce	87.8	87.9	93.0	105	90.6	100	91.1	62.2	76.5	98.4	62.2	89.0	93.7	62.5	94.3	90.4	102	97.2	84.5	81.2	62.4	66.4
Pr	10.6	10.3	11.3	12.6	10.7	12.1	11.0	7.93	9.17	11.8	7.87	10.5	11.2	8.02	11.3	11.1	12.4	11.5	10.1	9.75	8.17	8.66
Nd	42.6	42.7	46.1	50.4	42.9	48.9	44.8	35.0	38.7	46.7	34.3	44.3	45.7	34.7	47.1	44.5	50.9	45.9	41.1	40.1	37.7	38.6
Sm	9.27	9.13	9.74	10.6	8.85	10.0	9.18	8.23	8.19	9.52	7.81	9.00	9.59	7.56	9.66	9.16	10.7	9.26	8.72	8.37	9.11	10.1
Eu	3.09	2.99	3.22	3.36	3.03	3.26	2.97	2.73	2.83	3.14	2.66	2.97	3.17	2.55	3.20	3.18	3.46	3.00	2.82	2.79	2.93	3.45
Gd	8.61	8.14	9.19	10.1	8.47	9.47	8.73	7.96	7.84	8.97	8.02	8.34	9.19	7.91	9.24	8.87	10.1	8.71	8.14	7.99	8.82	10.6
Tb	1.15	1.16	1.30	1.29	1.18	1.26	1.16	1.16	1.02	1.17	1.07	1.11	1.24	1.09	1.26	1.26	1.35	1.13	1.12	1.08	1.30	1.56
Dy	6.57	6.21	7.15	7.24	6.39	7.03	6.57	6.41	5.72	6.33	5.91	6.53	6.72	6.06	7.15	6.92	7.66	6.46	6.28	5.90	7.06	9.26
Ho	1.14	1.06	1.28	1.26	1.12	1.22	1.09	1.12	1.10	1.16	1.07	1.09	1.22	1.11	1.18	1.24	1.32	1.15	1.12	1.08	1.20	1.65
Er	2.85	2.84	2.96	3.18	2.98	2.99	2.81	2.75	2.56	2.68	2.65	2.72	2.96	2.62	3.09	3.08	3.38	2.78	2.70	2.60	3.17	4.28
Tm	0.351	0.314	0.365	0.391	0.346	0.365	0.316	0.311	0.291	0.322	0.280	0.345	0.386	0.331	0.334	0.430	0.441	0.330	0.312	0.333	0.391	0.503
Yb	2.17	2.18	2.13	2.33	2.03	2.11	1.94	1.93	1.77	1.99	1.87	1.92	2.06	1.76	2.04	2.36	2.36	1.99	1.96	2.02	2.17	2.82
Lu	0.281	0.289	0.284	0.321	0.269	0.254	0.245	0.264	0.242	0.225	0.260	0.271	0.265	0.213	0.292	0.317	0.285	0.264	0.229	0.257	0.245	0.366

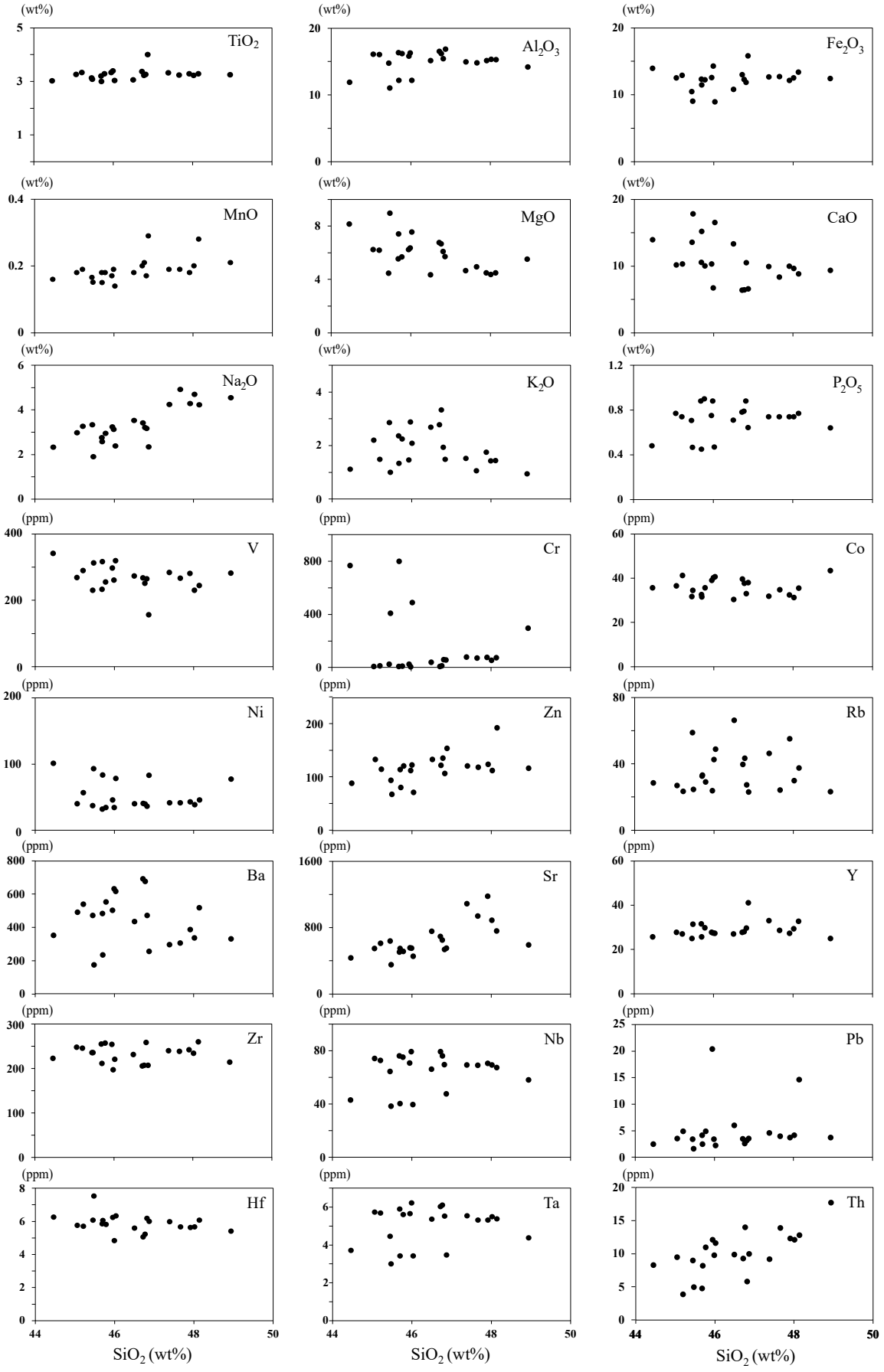

Fig. 6 Variation diagrams for the dolerite samples from the Uubulan area.

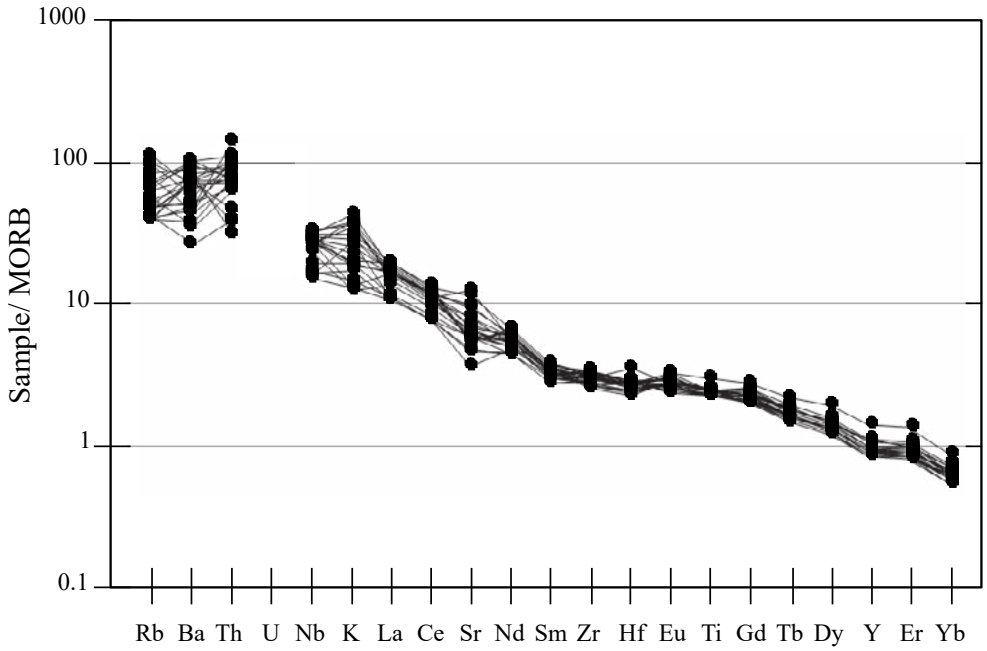

Fig. 7 Mid-ocean ridge basalt (MORB)-normalized multi-element patterns for the dolerite samples from the Uubulan area. The order of the elements follows Nakamura *et al*. (2000). The normalizing values are from Sun and MacDonald (1989).

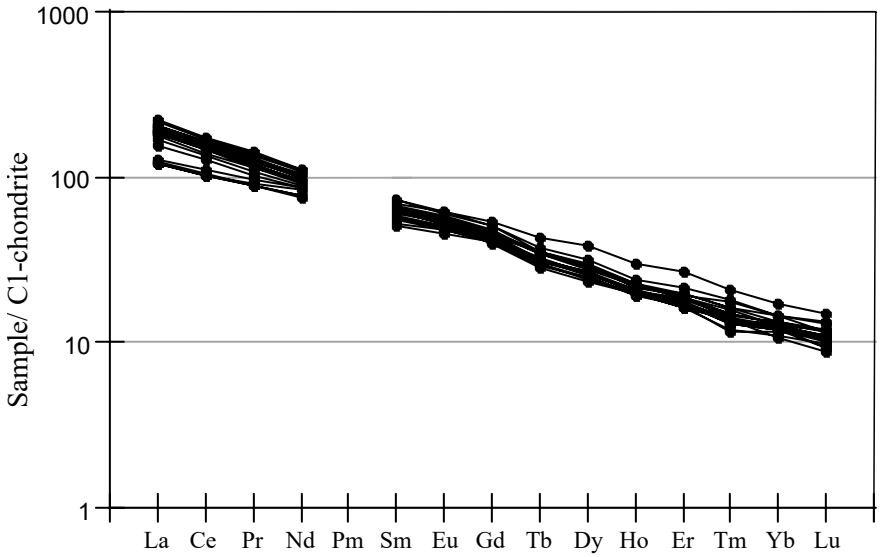

Fig. 8 C1-chondrite-normalized REE patterns for the dolerite samples from the Uubulan area. The normalizing values are from Anders and Grevesse (1989) and Yamamoto *et al*. (2005).

1.5 Cpx chemical composition of the mafic rocks

Representative mineral compositions of Cpx in the mafic rocks are listed in Table 2. The Cpx is assigned to augite and diopside in the pyroxene quadrilateral diagram (Morimoto, 1988) (Fig. 9). The Cpx chemical composition of each sample is described below.

Sample 2019615B6

Mg# (Mg/(Mg + Fe)) of Cpx is 0.60–0.65, 0.62 average, and was generally higher than that of sample

2019615B7. TiO_2 ranges from 3.09 to 5.38 wt%, Al_2O_3 varies from 7.62 to 11.1 wt% (10.2 wt% average), and CaO is 22.4–23.3 wt% (22.9 wt% average). Na_2O is less than 0.58 wt%.

Sample 2019615B7

The Cpx varies from 0.65 to 0.75 in Mg# (0.70 average). TiO_2 ranges from 1.53 to 3.68 wt% (2.58 wt% average), Al_2O_3 is 4.16 to 10.2 wt% (7.47 wt% average), and CaO is 21.0–22.4 wt% (21.8 wt% average). Na_2O is less than 0.54 wt%.

Sample 2019615B9

Mg# of Cpx is 0.51–0.62, 0.58 average. TiO_2 ranges from 1.9 to 3.9 wt%, Al_2O_3 varies from 5.16 to 10 wt% (7.1 wt% average), and CaO is 22.6–23.3 wt% (22.9 wt% average). Na_2O is less than 0.5 wt%.

Table 2 Representative mineral compositions of the clinopyroxene in the mafic rocks from the Uubulan area.

Sample No.	**2019615B6** Cpx (n=15)	**2019615B7** Cpx (n=30)	**2019615B9** Cpx (n=3)
SiO_2	41.8	45.4	44.6
TiO_2	4.25	2.58	2.65
Al_2O_3	10.2	7.49	7.10
Cr_2O_3	-	-	-
FeO*	10.5	9.60	12.4
MnO	-	-	-
MgO	9.80	12.7	9.84
CaO	22.9	21.9	22.9
Na_2O	0.490	0.354	0.47
Total	100.00	100.00	100.00
Mg#	0.624	0.701	0.585

The data are displayed to three significant digits.
FeO*is total iron as FeO.
Mg# (Mg/(Mg + Fe)) on molar basis.

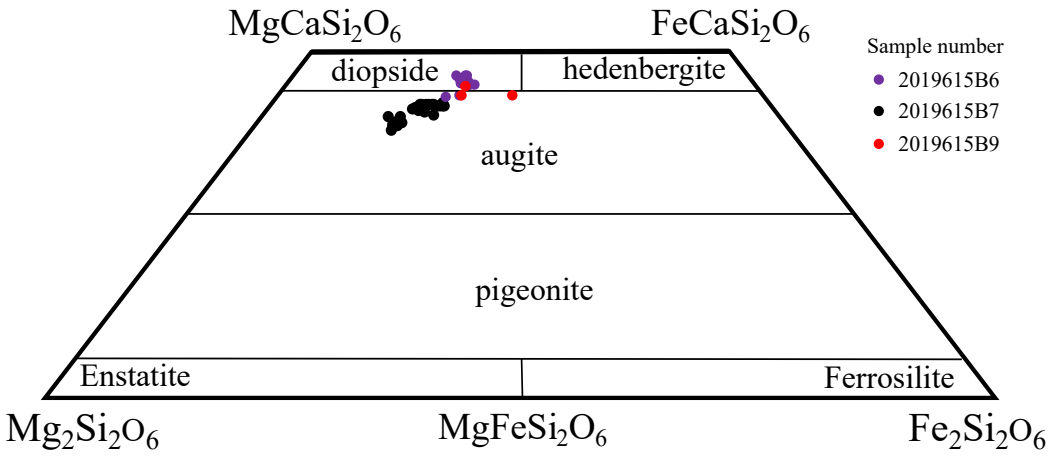

Fig. 9 Dolerite samples from the Uubulan area with their clinopyroxene chemical composition plotted on the pyroxene trapezoid.

Table 3 Results of the K-Ar dating. STP: standard temperature and pressure.

Sample No	Sample	K concentration (wt%)	Radioactive ^{40}Ar (10^{-8}cc STP/g)	K-Ar age (Ma)	Stable ^{40}Ar (%)
2019615B9	Hornblende	0.517 ± 0.010	930.3 ± 11.0	412.7 ± 8.6	14.7

1.6 Hornblende K-Ar age of the mafic rocks

The result of the hornblende K-Ar dating for the sample is shown in Table 3. K concentration is 0.517 ± 0.010 wt%, and radioactive ^{40}Ar is 930.4 ± 11.0 (10^{-8}cc (STP)/g); then the K-Ar age is calculated to be 412.7 ± 8.6 Ma. Analytical error under the same condition was less than 1% (Itaya *et al*., 1991; Yagi *et al*., 2015).

Discussion

1.7 Magma type and tectonic setting of the mafic rocks

The geochemistry of mafic rocks, which varies based on their origins, provides evidence for the volcanic activity that formed in the tectonic setting, and discrimination diagrams for mafic rocks have been proposed (Pearce, 1982). In this section, discrimination diagrams are used to discuss the magma type and tectonic setting of the mafic rocks in the Uubulan area.

The samples are plotted in the alkaline field, in ($Na_2O + K_2O$) vs. SiO_2, Nb/Y vs. SiO_2, and TiO_2 vs. $Zr/(P_2O_5 \times 10000)$ diagrams (MacDonald and Katsura, 1969; Winchester and Floyd, 1976, 1977) (Fig. 10a, b, and c). The samples show geochemical features similar to those of alkaline basalts, such as enriched LILE and LREE in comparison to the HFSE and HREE (Figs. 7 and 8). As observed from the Cpx chemical composition, all data fall on the field of alkaline basalt in Al vs. Si and Ti vs. (Ca + Na) diagrams (Leterrier *et al*., 1982) (Fig. 11a, b). Thus, the examined mafic rocks have an alkaline nature.

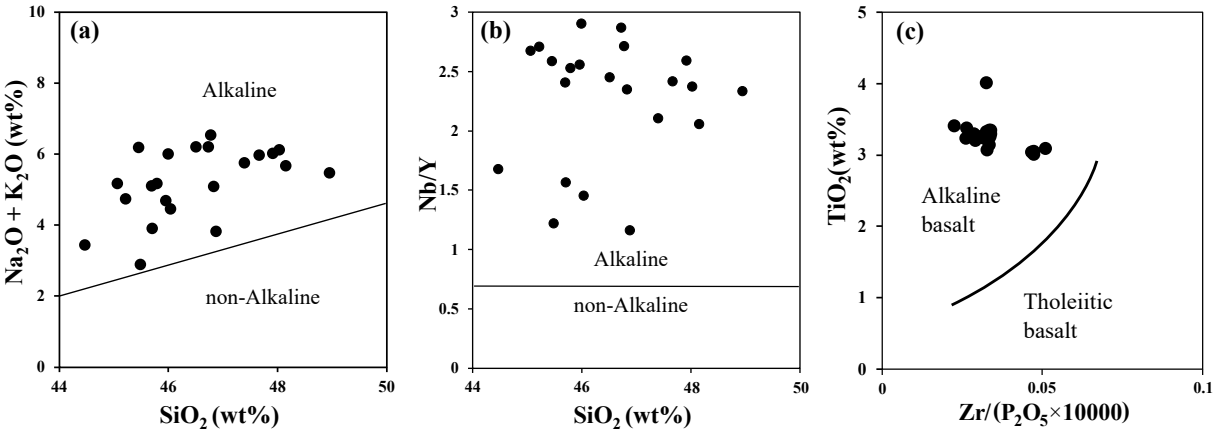

Fig. 10 Plot of the whole-rock chemical composition on the diagrams discriminating alkaline vs. non-alkaline mafic rocks for the dolerite samples from the Uubulan area: (a) ($Na_2O + K_2O$) vs. SiO_2 diagram from MacDonald and Katsura (1969); (b) Nb/Y vs. SiO_2 diagram from Winchester and Floyd (1977); (c) TiO_2 vs. $Zr/(P_2O_5 \times 10000)$ diagram from Winchester and Floyd (1976).

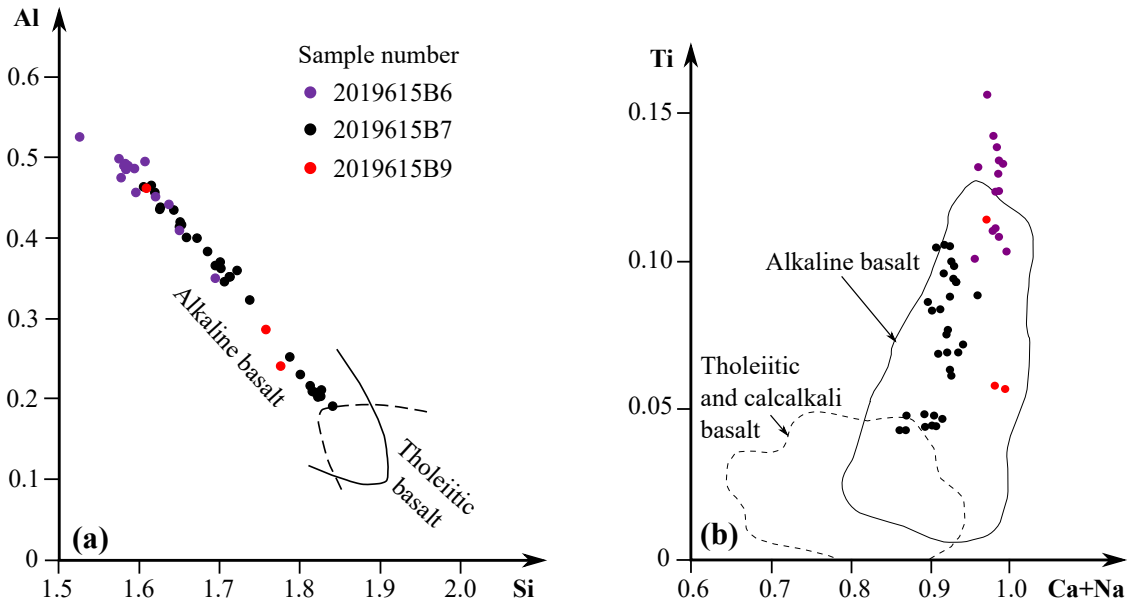

Fig. 11 The chemical composition of clinopyroxene in dolerite samples from the Uubulan area distinguishes between alkaline and non-alkaline (tholeiitic and calc-alkali) basalt: (a) Al vs. Si diagram (Leterrier *et al*., 1982); (b) Ti vs. (Ca + Na) diagram (Leterrier *et al*., 1982).

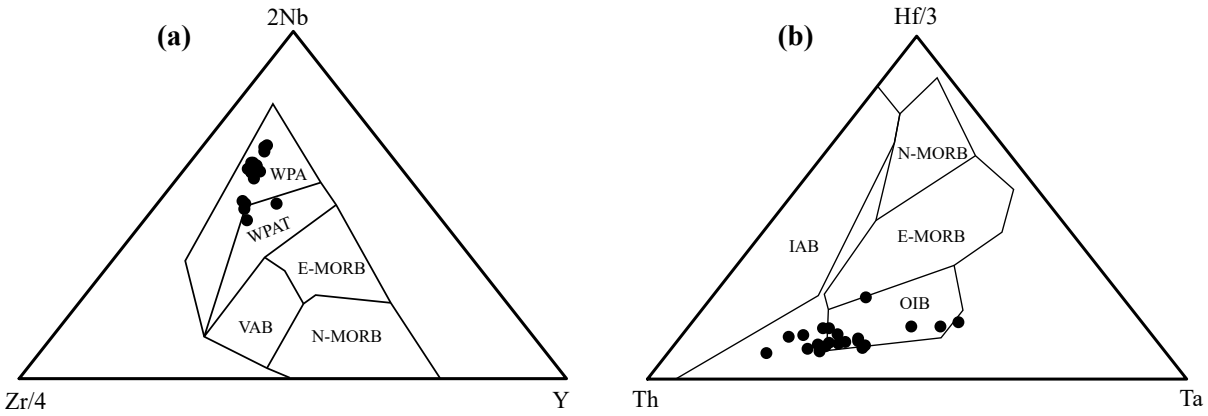

Fig. 12 Discrimination diagrams for the dolerite samples from the Uubulan area: (a) 2Nb–Zr/4–Y diagram (Meschede, 1986) and (b) Hf/3–Th–Ta diagram (Wood, 1980) show the fields for the different tectono-magmatic types. Abbreviations: WPA: within-plate alkaline; WPAT: within-plate alkaline and tholeiites; N-MORB: normal-type MORB; E-MORB: enriched-type MORB; VAB: volcanic arc-basalt; OIB: ocean-island basalt; IAB: island-arc basalt; BAB: back-arc basin basalts.

Zr/4–2Nb–Y diagram points that the samples were formed at a within-plate setting, and Th–Hf/3–Ta and HFSE vs. $(La/Yb)_{cn}$ diagrams suggest that the samples are oceanic island alkaline basalts (OIA) (Wood, 1980; Meschede, 1986; Nakamura *et al*., 2000) (Figs. 12 and 13). Therefore, it is quite probable that the mafic rocks from the Gorkhi Formation at the Uubulan area are OIA. Tsukada *et al*. (2013) studied the major and trace elemnent composition of the mafic rocks in the Uubulan area using XRF and suggested that these were OIA. The results of this study, detailed examination for trace elements including REE using ICP–MS, strongly supported Tsukada's view.

Four mantle end-members, i.e., depleted mantle (DM), high time-integrated μ ($^{238}U/^{204}Pb$) mantle (HIMU), enriched mantle I (EM I), and enriched mantle II (EM II), have been suggested for the mafic magma-source (Zindler

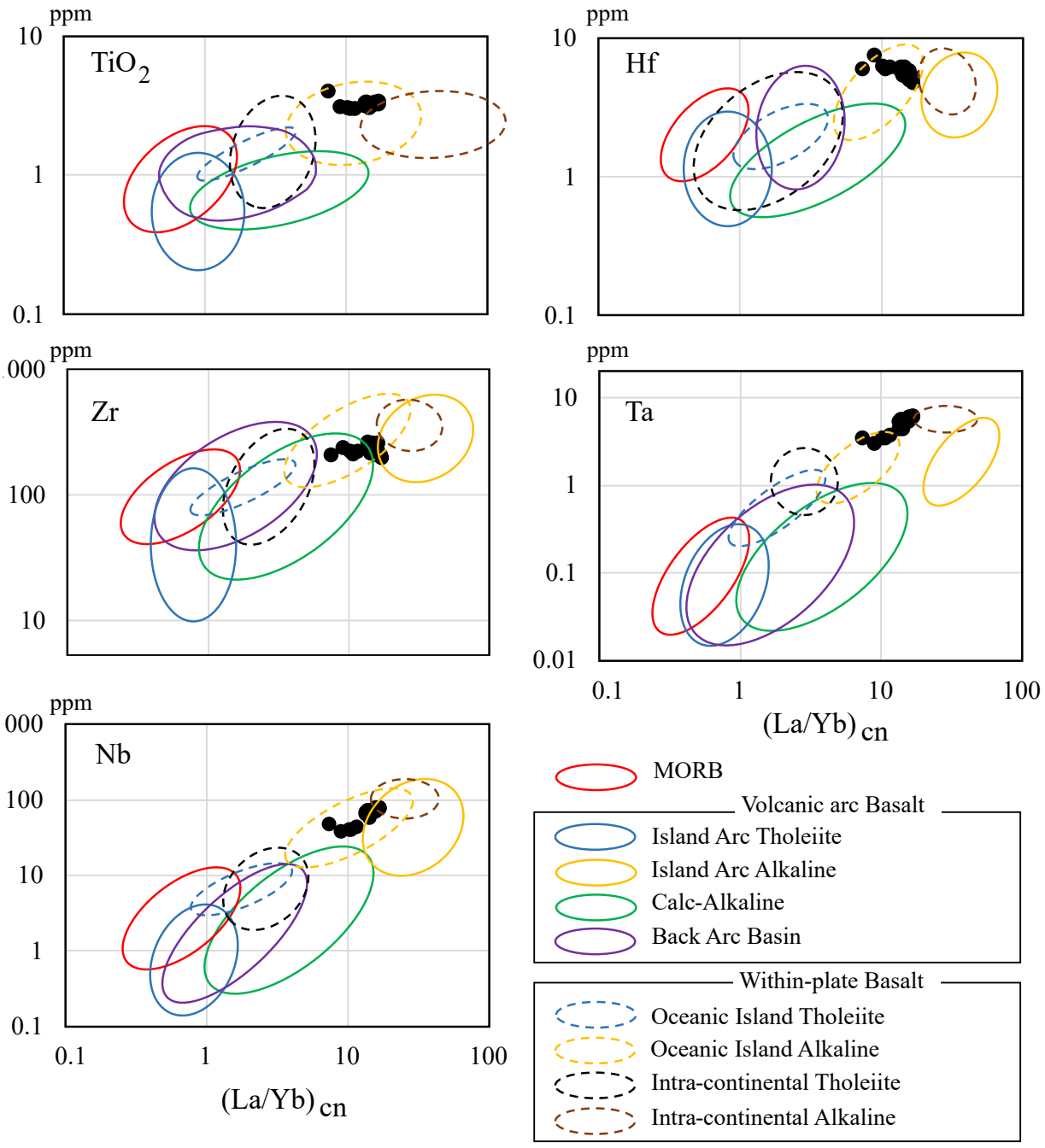

Fig. 13 Relationship between the concentration of high-field strength elements (HFSE) and the ratio of $(La/Yb)_{cn}$ in the dolerite samples from the Uubulan area. The diagrams are drawn based on the study by Nakamura *et al*. (2000).

and Hart, 1986). In plots of Th/Yb vs. Nb/Yb and TiO_2/Yb vs. Nb/Yb diagrams, the examined rocks show a strong affinity to the mafic rocks from St. Helena Island and Society Islands, which was originated from a HIMU source (Pearce, 2008) (Fig. 14a, b). The HIMU mafic rocks were known to show superplume activities (Kogiso *et al*., 1997; Homrighausen *et al*., 2018; Tominaga and Hara, 2021), and therefore, the present data, which shows trace elements composition similar to that of the HIMU mafic rocks, may imply the Late Silurian superplume activity at pelagic region. Further studies on $^{238}U/^{204}Pb$ (μ value), $^{232}Th/^{204}Pb$, and Pb isotopic ratios are required to confirm if the Uubulan rocks are of HIMU-origin.

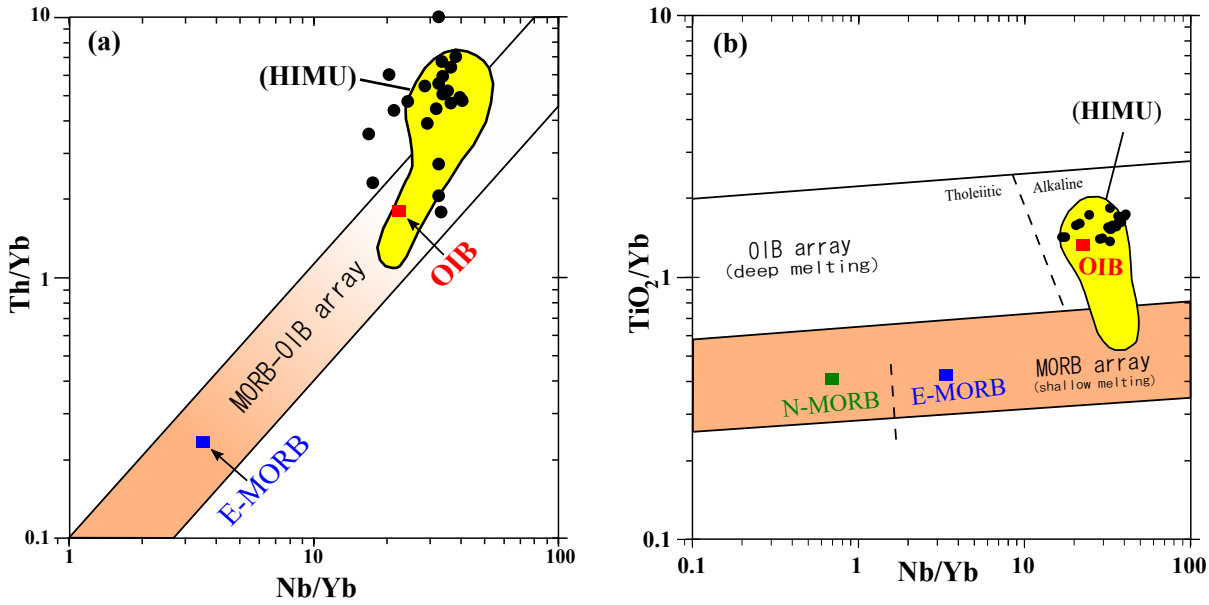

Fig. 14 Discrimination diagrams of (a) Th/Yb vs. Nb/Yb (Pearce, 2008) and (b) TiO_2/Yb vs. Nb/Yb (Pearce, 2008) for the dolerite samples from the Uubulan area. For comparison, the fields for HIMU lavas are shown. The data source of the HIMU lavas is Chaffey *et al*. (1989), Willbold and Stracke (2006), and Kawabata *et al*. (2011). Abbreviations: N-MORB: normal-type MORB; E-MORB: enriched-type MORB; OIB: ocean-island basalt; HIMU: high time-integrated μ ($^{238}U/^{204}Pb$) mantle.

1.8 Relationship between the mafic rocks and radiolarian chert at the Uubulan area

Upper Silurian (Ludlovian/Pridolian) chert is exposed beside the mafic rocks in the Uubulan area. Kurihara *et al*. (2009) mentioned that the mafic rocks are conformably overlain by gray tuffaceous chert and then overlain by the Ludlovian/Pridolian chert at this area. However, the exact age of the mafic rocks has not been presented.

Kurihara *et al*. (2009) described the latest Ludlovian to Pridolian or Pridolian conodonts, such as *Ozarkodina remscheidensis eosteinhornensis*, *Ozarkodina* sp., and *Belodella* sp., from the gray and red cherts beside the mafic rocks. The hornblende K-Ar age, 412.7 ± 8.6 Ma, for the mafic rocks here coincides with the conodont age of the chert within its error range, and thus, it supports the conformable relationship between the mafic rocks and Upper Silurian chert.

Considering the error range of the K-Ar dating, the mafic rocks might be of Early Devonian. However, as discussed below, the time of the accretion of the oceanic plate and its cover, a component of the Gorki Formation, is generally considered as Early Carboniferous (Kurihara *et al*., 2009; Hara *et al*., 2013). That is, the radiolarian chert at the Uubulan area, likely lithified after Early Carboniferous, had probably been presented on a bed of pelagic ocean as radiolarian ooze at the Early Devonian time. If the mafic magma intruded into or erupted on the hydrous unconsolidated/semi-consolidated Silurian radiolarian ooze, the magma quite likely brecciated because of rapid cooling by the surrounding water, and hyaloclastite, crumble breccia, pillow/autobrecciated lava, paragonite layers, and others should have been formed instead of the dolerite and gabbro exposed here. In reality, there is no evidence showing contact between magma and hydrous unconsolidated/semi-consolidated sediments in this area, and therefore, it is reasonable to suppose that the mafic rocks had already been formed before the radiolarian ooze-accumulation at the Late Silurian time.

Radiolarian assemblage suggesting Pragian to Emsian, including *Deflantrica sodium*, *Deflantrica* sp., *Pactarentinia* sp., *Palaeoscenidium* sp., and *Tlecerina horrida*, was recovered from the upper chert horizon of

the Upper Silurian chert (Kurihara *et al*., 2009). Consequently, an OIA mafic rocks and Upper Silurian to Lower Devonian radiolarian chert sequence is exposed at the Uubulan area.

1.9 Width of the Middle Paleozoic Ocean facing the "Siberian continent"

The OPS can provide key information regarding the continuous evolution of oceanic plates (Matsuda and Isozaki, 1991; Wakita and Metcalfe, 2005).

In this study, it is confirmed that the OIA mafic rocks are probably overlain by the Upper Silurian (Ludlovian/Pridolian) radiolarian chert in the Gorkhi Formation. The Lower to Upper Devonian radiolarian cherts were recovered from several sections of the Gorkhi Formation. The Upper Devonian (Frasnian) chert is overlain by siliceous mudstone and clastic rocks, and Kurihara *et al*. (2009) proposed reconstructed OPS, i.e., OIA mafic rocks, Upper Silurian–Upper Devonian radiolarian chert, and post-Devonian clastic rocks in ascending order, for the Gorkhi Formation.

Detrital zircons of 340–320 Ma were reported from the sandstone, which is the uppermost part of the OPS, of the Gorkhi Formation (Kelty *et al*., 2008; Bussien *et al*., 2011; Hara *et al*., 2013). Additionally, Takeuchi *et al*. (2012) described the Carboniferous (Visean) shallow marine formation, which probably unconformably overlaid the mafic rocks and chert of the Gorkhi Formation. These facts suggest that an oceanic island formed at the pelagic region in the Late Silurian time (Ludrovian/Pridorian) migrated toward a continent, accumulated deep-sea sediments on it during the movement, and reached the trench in the Early Carboniferous.

The time spent traveling the oceanic plate from ridge/oceanic island to trench can be estimated from the fossil record in the radiolarian chert between the mafic rocks and clastic rocks of the OPS. The accretionary complex of the Gorkhi Formation is regarded as a fossilized remain of the subducted oceanic plate beneath the "Siberian continent" (e.g., Onon and Tsukada, 2017). According to the radiolarian fossil record in the OPS of the Gorkhi Formation, the Middle Paleozoic oceanic plate facing the "Siberian continent" is estimated to have traveled from the Late Silurian to the Late Devonian for nearly 50 million years, from oceanic island to trench (Kurihara *et al*., 2009). The relative motion rate of the Pacific plate against the Eurasian eastern margin, which is a typical pair of the continent and subducted oceanic plate in Quaternary time, varies from 65 to 110 mm/yr, except for Eocene (Northrup *et al*., 1995). Assuming that the ancient oceanic plate subducted beneath the "Siberian continent" moved at a rate of 83 mm/yr, same as the current rate of the Pacific plate at 38°N, 144°E (DeMets *et al*., 1994), the distance from the oceanic island to the trench at Silurian–Devonian can be estimated to be approximately 4200 km. This is comparable to the distance from the Midway Islands in the central Pacific to the Japan Trench. As the oceanic island is located between ridge and trench, the ridge that generated the oceanic plate at Silurian–Devonian time had probably been located far more than the estimated distance here from the "Siberian continent."

Conclusion

(1) The mafic rocks of the Gorkhi Formation, Khangai-Daur belt at the Uubulan area show geochemical features similar to those of oceanic island alkaline basalt.

(2) The hornblende K-Ar age, 412.7 ± 8.6 Ma, from the mafic rocks here, coincides with the conodont age of the Upper Silurian chert exposed beside the mafic rocks within its error range. Therefore, the mafic rocks are very likely conformably overlain by the Upper Silurian chert.

(3) According to the OPS of the Gorkhi Formation (Kurihara *et al*., 2009), the mafic rocks at the Uubulan area had taken 50 million years to travel from an oceanic island to a trench along the margin of the "Siberian continent."

Assuming that the relative motion rate of the ancient oceanic plate subducted beneath the "Siberian continent" had been the same as the rate of the Pacific plate against the Eurasian eastern margin (83 mm/yr), the distance from the oceanic island to the trench at Silurian–Devonian time can be estimated to be approximately 4,200 km.

Acknowledgements

We would like to thank Dr. K. Yagi at the Hiruzen Institute for Geology and Chronology for his helpful advice. We are grateful to Prof. K. Yamamoto and Prof. Y. Asahara at Nagoya University for technical supports in XRF and ICP-MS analysis. We thank Dr. Y. Shimura at the Geological Survey of Japan and Dr. Onon. G at the Japan Gold K. K. for the helpful discussion. We would like to thank Profs. M. Takeuchi and H. Yoshida at Nagoya University for valuable advice. Special thank goes to Prof. Zorigtkhuu, D. and Prof. Purev, N. at the Mongolian University of Science and Technology for their help in using the university facilities. We are grateful to Dr. Oyunchimeg T. at the Institute of Geology, Mongolian Academy of Sciences, and Dr. S. Fujiwara at Nagoya University for their valuable comments on the manuscript. We would like to thank Enago (www.enago.jp) for the English language review. A part of this study was supported by the Daiko Foundation, Japan.

References

Anders, E. and Grevesse, N. (1989) Abundances of the elements: Meteoritic and solar. *Geochimica et Cosmochimica Acta*, **53**, 197–214.

Badarch, G. (2005) Tectonic overview of Mongolia. *Mongolian. Geoscientist*, **27**, 1–7.

Badarch, G., Cunningham, W.D., and Windley, B.F. (2002) A new terrane subdivision for Mongolia: implications for the Phanerozoic crustal growth of Central Asia. *Journal of Asian Earth Sciences*, **21**, 87–110.

Bulgatov, A. N. and Gordienko, I. V. (1999) Terranes, synaccretionary, and postaccretionary complexes of the Transbaikalia and southeastern part of Eastern Sayn Regions, Siberia. In: Nokleberg WJ, Naumova VV, Kuzmin MI, Bounaeva TV (ed) *Preliminary Publications Book 1 from Project on Mineral Resources, Metallogenesis, and Tectonics of Northeast Asia, Open-File Report, ser. 99–165*, 1–9. The United States Geological Survey, Reston.

Bussien, D., Gombojav, N., Winkler, W., and Quadt, A. (2011) The Mongol–Okhotsk Belt in Mongolia—an appraisal of the geodynamic development by the study of sandstone provenance and detrital zircons. *Tectonophysics*, **510**, 132–150.

Chaffey, D. J., Cliff, R. A., and Wilson, B. M. (1989) Characterization of the St Helena magma source. Geological Society, *London, Special Publications*, **42**, 257–276.

DeMets, C., Gordon, R. G., Argus, D. F., and Stein, S. (1994) Effect of recent revisions to the geomagnetic reversal time scale on estimates of current plate motions. *Geophysical Research Letters*, **21**, 2191–2194.

Dorjsuren, B., Bujinlkham, B., Minjin, Ch., and Tsukada, K. (2006) Geological setting of the Ulaanbaatar terrane in the Hangay-Hentey zone of the Devonian accretionary complex, central Mongolia. Tomurhuu, D., Natal'in, B. A., Ariunchimeg, Y., Khishigsuren, S., and Erdenesaikhan, G. (eds.) *Structural and Tectonic Correlation Across the Central Asia Orogenic Collage: Implications for Continental Growth and Intracontinental Deformation (Second International Workshop and Field Excursions for IGC Project 480), Abstract and Excursion Guidebook*, 39–42. Institute of Geology and Mineral Resources, Mongolian Academy of Sciences, Ulaanbaatar.

Gerel, O. and Lhamsuren, J. (1999) The Gorkhi Granite Pluton with miarolic pegmatites. *Excursion Guide, International Geological Symposium on East Asia*. Gerel, O. (2004) Magmatism and mineralization of the Granitic rocks in Mongolia. *Our Scientists*, **9**, 78–91. Mongolian University of Science and Technology, Ulaanbaatar.

Gordienko, I. V., Medvedev, A. Y., Gornova, M. A., Tomurtogoo, O., and Goneger, T. A. (2012) The Haraa Gol terrane in the western Hentiyn Mountains (northern Mongolia): geochemistry, geochronology, and geodynamics. *Russian Geology and Geophysics*, **53**, 281–292.

Hara, H., Kurihara, T., Tsukada, K., Kon, Y., Uchino, T., Suzuki, T., Takeuchi, M., Nakane, Y., Nuramkhaan, M., and Chuluun, M. (2013) Provenance and origins of a Late Paleozoic accretionary complex within the Khangai–Khentei belt in the Central Asian Orogenic Belt, central Mongolia. *Journal of Asian Earth Sciences*, **75**, 141–157.

Homrighausen, S., Hoernle, K., Geldmacher, J., Wartho, J. A., Hauff, F., Portnyagin, M., ... and Garbe-Schönberg, D. (2018) Unexpected HIMU-type late-stage volcanism on the Walvis Ridge. *Earth and Planetary Science Letters*, **492**, 251–263.

Itaya, T., Nagao, K., Inoue, K., Honjou, Y., Okada, T., and Ogata, A. (1991) Argon isotope analysis by a newly developed mass spectrometric system for K-Ar dating. *Mineralogical Journal*, **15**, 203–221.

Jahn, B. M., Windley, B., Natal'In, B., and Dobretsov, N. (2004) Phanerozoic continental growth in central asia. *Journal of Asian Earth Sciences*, **23**, 599–603.

Kawabata, H., Hanyu, T., Chang, Q., Kimura, J. I., Nichols, A. R., and Tatsumi, Y. (2011) The petrology and geochemistry of St. Helena alkali basalts: evaluation of the oceanic crust-recycling model for HIMU OIB. *Journal of Petrology*, **52**, 791–838.

Kelty, T. K., Yin, A., Dash, B., Gehrels, G. E., and Ribeiro, A. E. (2008) Detrital-zircon geochronology of Paleozoic sedimentary rocks in the Hangay–Hentey basin, north-central Mongolia: implications for the tectonic evolution of the Mongol–Okhotsk Ocean in central Asia. *Tectonophysics*, **451**, 290–311.

Kogiso, T., Tatsumi, Y., Shimoda, G., and Barsczus, H. G. (1997) High μ (HIMU) ocean island basalts in southern Polynesia: new evidence for whole mantle scale recycling of subducted oceanic crust. *Journal of Geophysical Research: Solid Earth*, **102**(B4), 8085–8103.

Kovalenko, V. I., Yarmolyuk, V. V., Kovach, V. P., Kotov, A. B., Kozakov, I. K., Salnikova, E. B., and Larin, A. M. (2004) Isotope provinces, mechanisms of generation and sources of the continental crust in the Central Asian mobile belt: geological and isotopic evidence. *Journal of Asian Earth Sciences*, **23**, 605–627.

Kurihara, T., Tsukada, K., Otoh, S., Kashiwagi, K., Minjin, C., Dorjsuren, B., Bujinlkham, B., Sersmaa, G., Manchuk, N., Niwa, M., Tokiwa, T., Hikichi, G., and Kozuka, T. (2009) Upper Silurian and Devonian pelagic deep-water radiolarian chert from the Khangai–Khentei belt of Central Mongolia: evidence for Middle Paleozoic subduction–accretion activity in the Central Asian Orogenic Belt. *Journal of Asian Earth Sciences*, **34**, 209–225.

Leterrier, J., Maury, R.C., Thonon, P., Girard, D., and Marchal, M. (1982) Clinopyroxene composition as a method of identification of the magmatic affinities of paleo-volcanic series. *Earth and Planetary Science Letters*, **59**, 139–154.

MacDonald, G. A. and Katsura, T. (1969) Chemical composition of Hawaiian Lavas. *Journal of Petrology*, **5**, 82–133.

Magic Project (1998) *Geologic Map of Ulan Bator, Scale 1:100,000*. Geological Information Center, Ulan Bator.

Matsuda, T. and Isozaki, Y. (1991) Well-documented travel history of Mesozoic pelagic chert in Japan: from remote ocean to subduction zone. *Tectonics*, **10**, 475–499.

Meschede, M. (1986) A method of discriminating between different types of mid-ocean ridge basalts and continental tholeiites with the Nb–Zr–Y diagram. *Chemical Geology*, **56**, 207–218.

Minjin, Ch., Tomurtogoo, O., and Dorjsuren, B. (2006) Devonian-Carboniferous accretionary complex of the Ulaanbaatar terrane. Tomurhuu, D., Natal'in, B.A., Ariunchimeg, Y., Khishigsuren, S., Erdenesaikhan, G. (eds.), *Structural and Tectonic Correlation Across the Central Asia Orogenic Collage: Implications for Continental Growth and Intracontinental Deformation (Second International Workshop and Field Excursions for IGC Project 480), Abstract and Excursion Guidebook*, 100–106. Institute of Geology and Mineral Resources, Mongolian Academy of Sciences, Ulaanbaatar.

Morimoto, N. (1988) Nomenclature of pyroxenes. *Mineralogy and Petrology*, **39**, 55–76.

Nagao, K., and Itaya, T. (1988) K-Ar age determination. *Memoir of Geological Society of Japan*, **29**, 5–21.

Nagao, K., Nishido, H., Itaya, T., and Ogata, K. (1984) An age determination by K-Ar method. *Bulletin of the Research Institute of Technology, Okayama University of Science*, **9**, 19–38.

Nakamura, K., Fujinaga, K., and Kato, Y. (2000) Rare earth element geochemistry of in-situ basalts from the Upper Cretaceous Shimanto belt and its implication for their origin. *Japanese Magazine of Mineralogical and Petrological Sciences,* **29**, 175–190.

Nakane, Y., Kurihara, T., Bakhat, N., Manchuk, N., Takeuchi, M., Tsukada, K., Sersmaa, G., and Khishigsuren, S. (2012) Geological division of the rocks at southeast of Ulaanbaatar (Gachuurt-Nalaikh), central Mongolia. *Bulletin of the Nagoya University Museum*, **28**, 19–26.

Northrup, C. J., Royden, L. H., and Burchfiel, B. C. (1995) Motion of the Pacific plate relative to Eurasia and its potential relation to Cenozoic extension along the eastern margin of Eurasia. *Geology*, **23**, 719–722.

Onon, G. (2017). Late Paleozoic low-angle southward-dipping thrust in the Züünharaa area, Mongolia: Implications for the tectonic process of the Central Asian Orogenic belt. *Doctoral Dissertation, Department of Earth and Environmental Sciences*. Nagoya University, Nagoya.

Onon, G. and Tsukada, K. (2017) Late Paleozoic low-angle southward-dipping thrust in the Züünharaa area, Mongolia: tectonic implications for the geological structures in the Sayan-Baikal and Hangai-Daur belts. *International Journal of Earth Sciences*, **106**, 2549–2573.

Pearce, J. A. (1982) Trace element characteristics of lavas from destructive plate boundaries. *Orogenic Andesites and Related Rocks*, 528–548.

Pearce, J. A. (2008) Geochemical fingerprinting of oceanic basalts with applications to ophiolite classification and the search for Archean oceanic crust. *Lithos*, **100**, 14–48.

Petrov, O. V., Pospelov, I.I., and Shokalsky, S. P. (2014) Legend and tectonic zoning of Northern, Central and Eastern Asia (Central Asian fold belt and adjacent tectonic structures). Petrov, O. V., Leonov, Y. G., and Pospelov, I. I. (eds.), *Tectonics of Northern, Central and Eastern Asia, Explanatory Note to the Tectonic map of Northern–Central–Eastern Asia and Adjacent Areas at scale 1:2 500 000. – SPb*., 18–32. VSEGEI Printing House, Leningrad.

Purevjav, N. and Roser, B. (2012) Geochemistry of Devonian–Carboniferous clastic sediments of the Tsetserleg terrane, Hangay Basin, Central Mongolia: provenance, source weathering, and tectonic setting. *Island Arc*, **21**, 270–287.

Ruppen, D., Knaf, A., Bussein, D., Winkler, W., Chimedtseren, A., and Quadt, A. (2013) Restoring the Silurian to Carboniferous northern active continental margin of the Mongol-Okhotsk Ocean in Mongolia: Hangay-Hentey accretionary wedge and seamount collision. *Gondwana Research*, **25**, 1517–1534.

Sengör, A. M. C., Natal'in, B. A., and Burtman, V. S. (1993) Evolution of the Altaid tectonic collage and Palaeozoic crustal growth in Eurasia. *Nature*, **364**, 299–307.

Sharav, D., Tsukada, K., Oyunchimeg, T., Manchuk, N., and Otgonbaatar, D. (2019) Quartz crystallinity of radiolarian chert in the Ulaanbaatar terrane. *Bulletin of Geology, Mongolia*, **61**, 186–193 (in Mongolian with English abstract).

Sun, S. S. and McDonough, W. F. (1989) Chemical and isotopic systematics of oceanic basalts: implications for mantle composition and processes. *Geological Society, London, Special Publications*, **42**, 313–345.

Takebe, M. and Yamamoto, K. (2003) Geochemical fractionation between porcellanite and host sediment. *The Journal of Geology*, **111**, 301–312.

Takeuchi, M., Tsukada, K., Suzuki, T., Nakane, Y., Sersmaa, G., Manchuk, N., Kondo, T., Matsuzawa, N., Bakhat, N., Khishigsuren, S., Onon, G., Katsurada, Y., Hashimoto, M., Yamasaki, S., Matsumoto, A., Oyu-Erdene, B., Bulgamtsemgel, M., Kundyz, S., Enkhchimeg, L., Ganzorig, R., Myagmarsuren, G., Jamiyandagva, O., and Molomjamts, M. (2012) Stratigraphy and geological structure of the Paleozoic system around Ulaanbaatar, Mongolia. *Bulletin of the Nagoya University Museum*, **28**, 1–18.

Tominaga, K. and Hara, H. (2021) Paleogeography of Late Jurassic large-igneous-province activity in the Paleo-Pacific Ocean: Constraints from the Mikabu greenstones and Chichibu accretionary complex, Kanto Mountains, Central Japan. *Gondwana Research*, **89**, 177–192.

Tomurtogoo, O. (2003). *Tectonic Map of Mongolia at the Scale of 1:1,000,000, and Tectonics of Mongolia (Brief Explanatory Notes to Tectonic Map of Mongolia at the scale of 1:1,000,000)*. Mineral Resources Authority of Mongolia, Ulaanbaatar.

Tomurtogoo, O. (2012) Tectonic subdivision of Mongolian orogenic domains. *Geological Institute Transaction*, **21**, 5–25 (in Mongolian).

Tomurtogoo, O., Byamba, J., Badarch, G., Minjin, C., Orolmaa, D., Khosbayar, P., and Chuluun, D. (1998) *Geologic Map*

of Mongolia, Scale 1: 1,000,000 and Summary. Mineral Resources Authority of Mongolia, Ulaanbaatar.

Tsukada, K. (2018) Quantitative analysis of chemical composition of anhydrous silicate minerals using SEM–EDX installed at Nagoya University Museum. *Bulletin of the Nagoya University Museum*, **34**, 1–10 (in Japanese).

Tsukada, K., Nakane, Y., Yamamoto, K., Kurihara, T., Otoh, S., Kashiwagi, K., Minjin, Ch., Sersmaa, G., Manchuk, N., Niwa, M., and Tokiwa, T. (2013) Geological setting of basaltic rocks in an accretionary complex, Khangai–Khentei belt, Mongolia. *Island Arc*, **22**, 227–241.

Tsukada, K., Purevsuren, N., Nuramkhaan, M., Gantumur, O., Hasegawa, H., and Yamamoto, K. (2018) Geochemistry of the Permian–Triassic volcano-plutonic rocks in the Oyut-uul area, northeast of Darkhan, Mongolia –Magmatism at southern margin of Siberian continent–. *Bulletin of the Nagoya University Museum*, **33**, 15–30.

Wakita, K. and Metcalfe, I. (2005) Ocean plate stratigraphy in East and Southeast Asia. *Journal of Asian Earth Sciences*, **24**, 679–702.

Willbold, M. and Stracke, A. (2006) Trace element composition of mantle end ‐ members: Implications for recycling of oceanic and upper and lower continental crust. *Geochemistry*, *Geophysics*, *Geosystems*, **7**, 1–30.

Winchester, J. A. and Floyd, P. A. (1976) Geochemical magma type discrimination; application to altered and metamorphosed basic igneous rocks. *Earth and Planetary Science Letters*, **28**, 459–469.

Winchester, J.A. and Floyd, P.A. (1977) Geochemical discrimination of different magma series and their differentiation products using immobile elements. C*hemcal Geology*, **20**, 325–345.

Windley, B. F., Alexeiev, D., Xiao, W., Kröner, A., and Badarch, G. (2007) Tectonic models for accretion of the Central Asian Orogenic Belt. *Journal of the Geological Society*, **164**, 31–47.

Wood, D. A. (1980) The application of a Th–Hf–Ta diagram to problems of tectonomagmatic classification and to establishing the nature of crustal contamination of basaltic lavas of the British Teriary volcanic province. *Earth and Planetary Science Letter*, **50**, 11–30.

Xiao, W., Windley, B. F., Hao, J., and Zhai, M. (2003) Accretion leading to collision and the Permian solonker suture, Inner Mongolia, China: termination of the central Asian orogenic belt. *Tectonics*, **22**, 1069.

Yagi, K., Okada, T., Honjou, Y., and Itaya, T. (2015) Argon analyses by isotopic dilution method using argon 38 spike with HIRU –Reproducibility and reliability in 25 years K-Ar dating. *Bulletin of the Research Institute of Technology, Okayama University of Science*, **33**, 42–52.

Yamamoto, K. and Morishita, T. (1997) Preparation of standard composites for the trace element analysis by X-ray fluorescence. *Journal of the Geological Society of Japan*, **103**, 1037–1045.

Yamamoto, K., Yamashita, F., and Adachi, M. (2005) Precise determination of REE for sedimentary reference rocks issued by the Geological Survey of Japan. *Geochemical Journal*, **39**, 289–297.

Zindler, A. and Hart, S. R. (1986) Chemical geodynamics. *Annual Review of Earth Planetary Sciences*, **14**, 493–571.

Zorin, Y. A. (1999) Geodynamics of the western part of the Mongolia–Okhotsk collisional belt, Trans-Baikal region (Russia) and Mongolia. *Tectonophysics*, **306**, 33–56.